CMS Physics Analysis Summary

Contact: cms-pag-conveners-b2g@cern.ch 2021/07/27

Search for resonant Higgs boson pair production in four b quark final state using large-area jets in proton-proton collisions at $\sqrt{s} = 13$ TeV

The CMS Collaboration

Abstract

A search is presented for pair production of the standard model Higgs boson using data from proton-proton collisions at a centre-of-mass energy of 13 TeV, collected by the CMS experiment at the CERN LHC in 2016−2018, corresponding to an integrated luminosity of 138 fb^{-1}. The final state consists of two b quark-antiquark pairs. The search is conducted in the region of phase space where at least one of the pairs is highly Lorentz-boosted and is reconstructed as a single large-area jet. The other pair may be either similarly boosted or resolved, the latter reconstructed using two b-tagged jets. The data was found to be consistent with the measured standard model processes. Limits in the range 9.74−0.29 fb and 4.94−0.19 fb were set on the product of the cross sections and the branching fractions of the spin-0 radion and the spin-2 bulk graviton with a mass of 1−3 TeV, respectively, in the context of warped extradimensional models.

1 Introduction

In proton-proton (pp) collisions at the CERN Large Hadron Collider (LHC), the standard model (SM) production of a pair of Higgs bosons [1–3] involves the gluon fusion and an internal fermion loop dominated by the top quark, t. Its cross section of $33.5^{+2.5}_{-2.8}$ fb at a centre-of-mass energy of 13 TeV [4–6], is too small to be observable with the current data. However, according to many beyond the standard model (BSM) theories, other modes of Higgs boson pair production could exist, many involving the production of a massive BSM resonance X that then decays to a Higgs boson pair ($X \to HH$) [7]. Even for resonance mass m_X too large for X to be directly produced in pp interactions, the particle could manifest itself through off-shell effects, leading to anomalous couplings of the H boson to the SM particles, including the HH self-interaction [8]. Thus, BSM effects may modify the HH differential and integral production cross sections, making this process observable with current data.

Models with a warped extra dimension (WED), as proposed by Randall and Sundrum [7], are among those BSM scenarios that predict the existence of resonances with large couplings to the SM Higgs boson, such as the spin-0 radion [9–11] and the spin-2 first Kaluza–Klein (KK) excitation of the graviton [12–14]. The WED models [15] postulate an additional spatial dimension l compactified between two four-dimensional hypersurfaces known as the branes, with the region between, the bulk, warped by an exponential metric κl, where κ is the warp factor. A value of $\kappa l \sim 35$ fixes the mass hierarchy between the Planck scale M_{Pl} and the electroweak scale [7]. One of the parameters of the model is $\kappa/\overline{M_{Pl}}$, where $\overline{M_{Pl}} \equiv M_{Pl}/\sqrt{8\pi}$. The ultraviolet cutoff scale of the model $\Lambda_R \equiv \sqrt{6}e^{-\kappa l}\overline{M_{Pl}}$ [9] is another parameter, and is expected to be near the TeV scale.

Searches for HH production have been performed by the ATLAS [16–22] and CMS [23–31] Collaborations using the LHC pp collision data at $\sqrt{s} = 8$ and 13 TeV. A search targeting the high m_X range for a KK bulk graviton or a radion decaying to HH, in the $b\bar{b}b\bar{b}$ final state, was published by the CMS Collaboration [32], in which two large-area jets are used to reconstruct the highly Lorentz-boosted Higgs bosons ("fully-merged" event topology). A similar search, focusing on a lower range of m_X, was also performed by CMS [33], using events with four separate b quark jets. The configuration of a Higgs boson candidate as one large-area jet or as two separate smaller jets is dependent on the momentum of the Higgs boson [34].

In this note, we improve upon the CMS search for high mass resonance ($1000 \leq m_X \leq 3000$ GeV) decaying to $HH \to b\bar{b}b\bar{b}$ [35] by using full Run 2 data corresponding to an integrated luminosity of 138 fb^{-1}. Owing to the broad mass range explored, the $H \to b\bar{b}$ decay is reconstructed using two techniques for two separate analysis channels. In the first, it is assumed that both Higgs bosons are highly Lorentz-boosted and are reconstructed using large-area jets ("fully-boosted" channel). In the second, the more boosted Higgs boson is reconstructed using a large-area jet and the other is reconstructed from two separate b quark jets ("semi-resolved" channel). The inclusion of the semi-resolved events leads to a significant improvement in the search sensitivity for resonances with $1000 \leq m_X \leq 2000$ GeV.

This note is organized as follows: a brief description of the CMS detector is given in Section 2 followed by a description of event simulation in Section 3. The event selection criteria are defined in Section 4 after which Section 5 describes the modelling of the major background processes. These are followed by Section 6 on the relevant systematic uncertainties and Section 7 where the results are presented. The search is summarized in Section 8.

2 The CMS detector and event reconstruction

The central feature of the CMS apparatus is a superconducting solenoid of 6 m internal diameter, providing a magnetic field of 3.8 T. Within the solenoid volume are a silicon pixel and strip tracker, a lead tungstate crystal electromagnetic calorimeter (ECAL), and a brass and scintillator hadron calorimeter (HCAL), each composed of a barrel and two endcap sections. Forward calorimeters, made of steel and quartz-fibres, extend the pseudorapidity (η) coverage provided by the barrel and endcap detectors. Muons are detected in gas-ionization chambers embedded in the steel flux-return yoke outside the solenoid. A more detailed description of the CMS detector, together with a definition of the coordinate system used and the relevant kinematic variables, can be found in Ref. [36].

Events of interest are selected using a two-tiered trigger system [37]. The first level (L1), composed of custom hardware processors, uses information from the calorimeters and muon detectors to select events at a rate of around 100 kHz within a time interval of less than 4 μs. The second level, known as the high-level trigger, consists of a farm of processors running a version of the full event reconstruction software optimised for fast processing, and reduces the event rate to around 1 kHz before data storage [38].

The particle-flow algorithm [39] (PF) aims to reconstruct and identify each individual particle in an event (PF candidate), with an optimized combination of information from the various elements of the CMS detector. The energy of photons is obtained from the ECAL measurement. The energy of electrons is determined from a combination of the track momentum at the main interaction vertex, the corresponding ECAL cluster energy, and the energy sum of all bremsstrahlung photons attached to the track. The momentum of muons is obtained from the curvature of the corresponding track. The energy of charged hadrons is determined from a combination of their momentum measured in the tracker and the matching ECAL and HCAL energy deposits, corrected for zero-suppression effects and for the response function of the calorimeters to hadronic showers. Finally, the energy of neutral hadrons is obtained from the corresponding corrected ECAL and HCAL energies.

For each event, jets are clustered from these reconstructed particles using the infrared and collinear safe anti-k_{T} algorithm [40, 41] with a distance parameter of 0.4 (AK4 jets) or 0.8 (AK8 jets). Jet momentum is determined as the vectorial sum of all particle momenta in the jet, and is found from simulation to be, on average, within 5 to 10% of the true momentum over the whole transverse momentum (p_{T}) spectrum and detector acceptance. Additional pp interactions within the same or nearby bunch crossings can contribute additional tracks and calorimetric energy depositions, increasing the apparent jet momentum. To mitigate this effect, tracks identified to be originating from pileup vertices are discarded and an offset correction is applied to correct for remaining contributions. Jet energy corrections are derived from simulation studies so that the average measured energy of jets becomes identical to that of particle level jets. In situ measurements of the momentum balance in dijet, photon+jet, Z+jet, and multijet events are used to determine any residual differences between the jet energy scale in data and in simulation, and appropriate corrections are made [42]. Additional selection criteria are applied to each jet to remove jets potentially dominated by instrumental effects or reconstruction failures. The jet energy resolution amounts typically to 15–20% at 30 GeV, 10% at 100 GeV, and 5% at 1 TeV [42].

The missing transverse momentum vector $\vec{p}_{\mathrm{T}}^{\,\mathrm{miss}}$ is computed as the negative vector sum of the transverse momenta of all the PF candidates in an event, and its magnitude is denoted as $p_{\mathrm{T}}^{\mathrm{miss}}$ [43]. The $\vec{p}_{\mathrm{T}}^{\,\mathrm{miss}}$ is modified to account for corrections to the energy scale of the reconstructed jets in the event.

3 Event simulation

The bulk graviton and radion signal events are simulated at leading order in the mass range 1000–3000 GeV with a width of 1 MeV (much smaller than experimental resolution), using the MADGRAPH5_aMC@NLO 2.3.3 [44] event generator. The NNPDF3.0 leading order parton distribution function (PDF) set [45], taken from LHAPDF6 PDF set [46–49], with the four-flavour scheme, is used. The showering and hadronization of partons are simulated with PYTHIA 8.212 [50].

The dominant background consists of events comprised uniquely of jets (multijet events) arising from the SM quantum chromodynamics (QCD) interaction, and is modelled entirely from data. The remaining background, consisting mostly of $\mathrm{t\bar{t}}$+jets events, is modelled using POWHEG 2.0 [51–53] and interfaced to PYTHIA 8. The CUETP8M2T4 tune [54, 55] is used for generating the $\mathrm{t\bar{t}}$+jets events. The $\mathrm{t\bar{t}}$+jets background rate is estimated using a next-to-next-to-leading order cross section of 832^{+46}_{-52} pb [56], corresponding to the top quark mass of 172.5 GeV. A sample of multijet events from QCD interactions, simulated at leading order using MADGRAPH5_aMC@NLO and PYTHIA 8, is used to develop and validate the background estimation techniques, prior to being applied to the data.

All generated samples were processed through a GEANT4-based [57, 58] simulation of the CMS detector. The effect of pileup, averaging to 23–30 at the LHC beam conditions between 2016–2018, is included in the simulations, and the samples are reweighted to match the distribution of the number of pp interactions observed in the data, assuming a total inelastic pp collision cross section of 69.2 mb [59].

4 Event selection

Collision events are selected using a combination of triggers based on the jet activity in the event. An event is selected if the scalar sum of the p_T of all AK4 jets in the event (H_T) is greater than 800, 900, or 1050 GeV, depending on the data collection year and the LHC beam instantaneous luminosity. Events with $H_\mathrm{T} \geq 650$ GeV, a pair of jets with invariant mass above 900 GeV, and a pseudorapidity separation $|\Delta\eta| < 1.5$ are also selected. A third HLT trigger accepts events if the p_T of the leading AK8 jets is greater than 360 or 400 GeV and the "trimmed mass" of an AK8 jet is above 30 GeV. The jet trimmed mass is obtained after removing remnants of soft radiation with the jet trimming technique [60], using a subjet size parameter of 0.3 and a subjet-to-AK8 jet p_T fraction of 0.1.

Jets in events collected using the logical OR of the above HLT triggers are required to have $|\eta| < 2.4$, and $p_\mathrm{T} > 30$ GeV for AK4 jets and $p_\mathrm{T} \geq 300$ GeV for AK8 jets. One AK8 jet is used to identify a boosted and spatially merged $\mathrm{H} \to \mathrm{b\bar{b}}$ decay (H jets) while two AK4 jets are used to reconstruct a spatially resolved $\mathrm{H} \to \mathrm{b\bar{b}}$ decay.

Initial step in the event selection requires the subleading AK8 jet to have a soft-drop mass [61, 62] between 110 and 140 GeV, consistent with the measured mass of the Higgs boson $m_\mathrm{H} = 125.09$ GeV. This selection corresponds to an efficiency of about 60–70% for a resonant signal mass m_X in the range 1000–3000 GeV.

The merged $\mathrm{H} \to \mathrm{b\bar{b}}$ jet is identified using a deep neural-network-based tagger, "DeepAK8". We use the "mass decorrelated" version of this tagger, which does not sculpt the jet mass in the multijet background events, since this variable is used in the background estimation procedure. The DeepAK8 tagger outperforms the previously used "double-b" $\mathrm{H} \to \mathrm{b\bar{b}}$ tagger, resulting in an increase of the search sensitivity of about 2.5 over the whole search domain.

For selecting signal event candidates, the DeepAK8 discriminator of the AK8 jets must be above 0.8 (loose criterion) or above 0.9 (tight criterion). The fully-boosted channel contains two "signal regions" (SR), defined using the DeepAK8 discriminator: events are categorized as either tight-tight (TT), where both AK8 jets pass the tight threshold, or as loose-loose (LL) otherwise. We denote the signal regions as "pass" regions. For the purpose of background estimation, for each signal region we also define a control region where the leading jet failed the tagging requirement; we denote them as "fail" regions. The fail region for TT SR is defined by leading H-jet failing but the subleading passing the tight criterion. Analogously, the fail region for LL SR is defined by the leading H-jet failing the loose criterion while the subleading passing it. This allows modeling of the signal regions using the fail regions that have the same criteria for the subleading jet as the corresponding signal regions they are used to predict. It also ensures that the fail regions for TT and LL signal regions are mutually exclusive.

Two dedicated $\mathrm{t\bar{t}}$ categories are also used in order to constrain the modelling of the $\mathrm{t\bar{t}}$+jets background component for events with larger jet p_{T}, for which the usual $\mathrm{t\bar{t}}$ measurements cease to be applicable. The $\mathrm{t\bar{t}}$ control regions use the same selections as TT and LL categories, with the exception of window on the soft-drop mass of the subleading jet, which is shifted from $110 < m_{SD} < 140$ to $140 < m_{SD} < 210$ in order to capture the top peak. This provides an *in situ* measurement of the top re-weighting uncertainty which is used in the full likelihood fit.

To find a Higgs boson decay into two resolved b quark jets, all AK4 jets in each event are examined for their b tag value using "DeepJet" algorithm, which gives the probability of a jet to have originated from the hadronization of a bottom quark. DeepJet is a deep neural network, trained using information from tracks and secondary vertices associated to the jets. The DeepJet requirement on AK4 jets corresponds to a 1% mistag rate for light flavoured jets. The resulting b-tagging efficiency is about 70% for b quark jets in the p_{T} range 80–150 GeV, and decreases to about 50% for $p_{\mathrm{T}} \sim 1000$ GeV. The b tagging efficiency in the simulations is corrected to match the one in the data, using measurements of the b tagging algorithm performance in a sample of muon-tagged jets and b jets from $\mathrm{t\bar{t}}$+jets events, where the correction factor ranges from approximately 0.95 to 1.1.

Resolved $\mathrm{H} \to \mathrm{b\bar{b}}$ candidates are identified by examining all pairs of b-tagged AK4 jets. Events are required to have least one pair where both AK4 jets are $\Delta R > 0.8$ away from the leading-p_{T} AK8 jet and within $\Delta R < 1.5$ of each other. If several such pairs are found, the pair of jets, j_1 and j_2, that has the highest sum of the AK4 jet DeepJet discriminator values is selected. The leading-p_{T} AK8 jet is then identified as the boosted H candidate, and the pair of AK4 jets is identified as the resolved H candidate. If no pairs are found, this process is repeated with the subleading-p_{T} AK8 jet. If a pair of AK4 jets is identified, then the subleading-p_{T} AK8 jet is identified as the boosted H candidate, and the pair of AK4 jets is identified as the resolved H candidate. If no pairs are found once again, the event is rejected. The invariant mass of j_1 and j_2, $m_{\mathrm{JJ}}(\mathrm{j}_1, \mathrm{j}_2)$, is required to be within 90–140 GeV, forming the resolved $\mathrm{H} \to \mathrm{b\bar{b}}$ candidate. For the semi-resolved channel, the signal region used for background estimation requires the AK8 jet to pass the DeepAK8 tight requirement and the anti-tag region to fail the tight requirement.

A resonant HH signal of high mass results in a small pseudorapidity separation between the two Higgs bosons, while the candidates from the multijet background typically have a larger pseudorapidity separation. Events in the fully-boosted channel are therefore required to have a pseudorapidity difference between the two H jets, $|\Delta\eta| < 1.3$. No such criterion is applied to the semi-resolved channel.

The main variable used in the search for a HH resonance is the "reduced mass". The fully-boosted analysis, it is defined as $m_{\mathrm{red}} \equiv m_{\mathrm{JJ}} - (m_{\mathrm{J}} - m_{\mathrm{H}}) - (m_{\mathrm{J}_2} - m_{\mathrm{H}})$, where m_{J} and m_{J_2}

are the soft-drop masses of the leading and subleading H-tagged jets in the event, and $m_{\mathrm{H}} = 125.09\,\mathrm{GeV}$ [63, 64] is the Higgs boson mass. In the semi-resolved analysis, this quantity is defined by $m_{\mathrm{red}} \equiv m_{\mathrm{Jjj}} - (m_{\mathrm{J}} - m_{\mathrm{H}}) - (m_{\mathrm{JJ}}(\mathrm{j}_1,\mathrm{j}_2) - m_{\mathrm{H}})$. The reduced mass is used rather than the invariant mass of the two reconstructed $\mathrm{H} \to \mathrm{b\bar{b}}$ decays because by subtracting the reconstructed masses of the two $\mathrm{H} \to \mathrm{b\bar{b}}$ candidates and adding back the measured Higgs boson mass m_{H}, fluctuations caused by jet energy and mass resolutions are mitigated, leading to 8–10% improvement in the dijet mass resolution. A requirement of $m_{\mathrm{red}} > 750\,\mathrm{GeV}$ is applied for selecting signal-like events.

Table 1: Event selection for the fully-merged topology.

Variable	Selection
Leading two AK8 jets	$p_{\mathrm{T}} > 300\,\mathrm{GeV}$ and $\lvert\eta\rvert < 2.4$
$\Delta\eta_{jj}$	< 1.3
Sub-leading AK8 jet soft-drop mass	$110 < m_{SD} < 140$
m_{red}	> 750

Table 2: Event selection for the semi-resolved topology.

Variable	Selection
Leading AK8 jet	$p_{\mathrm{T}} > 300\,\mathrm{GeV}$ and $\lvert\eta\rvert < 2.4$
Leading AK4 jets	$p_{\mathrm{T}} > 30\,\mathrm{GeV}$ and $\lvert\eta\rvert < 2.4$
$\Delta\eta_{jjj}$	< 1.3
DeepJet	Medium Working Point
Invariant combined AK4 soft-drop mass	$90 < m_{SD} < 140$
m_{red}	> 750

5 Background estimation

The two dominant sources of the standard model background are the multijet production and $\mathrm{t\bar{t}}$+jets. Both backgrounds are estimated in data, but the procedure is assisted by simulations. The multijet background estimation relies on the ratio of events that pass and fail the DeepAK8 Higgs tagger selection on the leading jet. This ratio is predicted by the simulation, but a correction factor is fitted in low and high sidebands of m_{J} and is interpolated through the signal region to predict the multijet event yield as a function of m_{red}. The $\mathrm{t\bar{t}}$ component is modeled well by the simulation and is obtained by fitting simulation templates to data in the whole $(m_{\mathrm{J}}, m_{\mathrm{red}})$ plane and by simultaneously fitting the $\mathrm{t\bar{t}}$ control region.

A likelihood fit to data is used to test the signal hypothesis. The total background model is constructed as a sum of the individual background contributions using a Poisson distribution for each bin of the $(m_{\mathrm{J}}, m_{\mathrm{red}})$ distribution. We compare the number of expected events from both the background-only and signal-plus-background hypotheses with the number of observed events in data.

The expected number of signal events is calculated as $N_{\mathrm{expected}} = \sigma_{\mathrm{X}}\mathcal{B}(\mathrm{X} \to \mathrm{HH} \to 4\mathrm{b})\varepsilon L$, where σ_{X} the production cross section of X (a radion or a bulk graviton), $\mathcal{B}(\mathrm{X} \to \mathrm{HH} \to 4\mathrm{b})$ is the product of the branching fraction of $\mathrm{X} \to \mathrm{HH}$ and the square of the branching ratio of $\mathrm{H} \to \mathrm{b\bar{b}}$, ε is the product of the acceptance and the efficiency to reconstruct a HH event with at least one boosted Higgs jet, and L is the integrated luminosity of the data set.

The number of expected events failing, n_F, and passing, n_P, DeepAK8 Higgs jet tagging in a given bin is given by

$$n_F(i,\vec{\theta}) = n_F^{\mathrm{QCD}}(i) + n_F^{\mathrm{t\bar{t}}}(i,\vec{\theta}) + n_F^{\mathrm{X}}(i,\vec{\theta})$$

and

$$n_P(i,\vec{\theta}) = n_P^{\mathrm{QCD}}(i) + n_P^{\mathrm{t\bar{t}}}(i,\vec{\theta}) + n_P^{\mathrm{X}}(i,\vec{\theta})$$

where i is a bin in the two-dimensional $(m_{\mathrm{J}}, m_{\mathrm{red}})$ plane, and $\vec{\theta}$ is the set of all nuisance parameters that quantify the systematic uncertainties, as described in Sec. 6. Each bin in the "fail" two-dimensional distribution, $n_F^{\mathrm{QCD}}(i)$ is represented by an individual fit parameter that is required to be positive but is otherwise unconstrained.

Lastly, the predicted multijet yield in the "pass" two-dimensional distribution, $n_P^{\mathrm{QCD}}(i)$ is obtained by

$$n_P^{\mathrm{QCD}}(i) = n_F^{\mathrm{QCD}}(i) R_{P/F}(m_{\mathrm{J}}, m_{\mathrm{red}})$$

where $R_{P/F}(m_{\mathrm{J}}, m_{\mathrm{red}})$ is a transfer function. We define the ratio of the multijet background distributions that pass and fail the Higgs tagging requirement in data and QCD multijet MC simulation as $R_{P/F}^{\mathrm{data}}(m_{\mathrm{J}}, m_{\mathrm{red}})$ and $R_{P/F}^{\mathrm{MC}}(m_{\mathrm{J}}, m_{\mathrm{red}})$, respectively.

Because of the combinatorial nature of multijet processes, $R_{P/F}^{\mathrm{data}}(m_{\mathrm{J}}, m_{\mathrm{red}})$ and $R_{P/F}^{\mathrm{MC}}(m_{\mathrm{J}}, m_{\mathrm{red}})$ are both smooth as a function of m_{J} and m_{red}. The data-to-simulation ratio of these two-dimensional functions (denoted by $R_{\mathrm{ratio}}(m_{\mathrm{J}}, m_{\mathrm{red}})$) is thus also smooth, and can be parameterized with an analytic function of m_{J} and m_{red}.

While $R_{P/F}^{\mathrm{data}}(m_{\mathrm{J}}, m_{\mathrm{red}})$ could also be described by analytic functions, features of this shape that are hard to model analytically can be factored out by using the QCD MC simulation, and the fit of the analytic function to data is only responsible for describing the residual differences between data and simulation that can be parameterized with fewer parameters than the shape of $R_{P/F}^{\mathrm{data}}(m_{\mathrm{J}}, m_{\mathrm{red}})$.

Thus the number of events in a given bin of the passing region is obtained from

$$n_P^{\mathrm{QCD}}(i) = n_F^{\mathrm{QCD}}(i) R_{P/F}^{\mathrm{MC}}(m_{\mathrm{J}}, m_{\mathrm{red}}) R_{\mathrm{ratio}}(m_{\mathrm{J}}, m_{\mathrm{red}})$$

where $R_{\mathrm{ratio}}(m_{\mathrm{J}}, m_{\mathrm{red}})$ is a surface parameterized by the product of two one-dimensional polynomials in the $(m_{\mathrm{J}}, m_{\mathrm{red}})$ plane with coefficients determined from the fit to data. Based on the Fisher test, where polynomial terms were added until the p-value obtained in the test was less than 0.95, a second-order polynomials were chosen for both m_{J} and m_{red} axes.

To reduce the effect of statistical fluctuations on the calculation of $R_{P/F}^{\mathrm{MC}}(m_{\mathrm{J}}, m_{\mathrm{red}})$ in the QCD multijet simulation, the pass and fail distributions are smoothed by using an adaptive kernel density estimate (KDE)[65]]prior to calculating the ratio. The smoothing has been repeated for several values of the "bandwidth" parameter of the KDE algorithm, which acts as a scale for the width of the adaptive kernels. The nominal value is 7 for all regions, except for the TT region which has a nominal value of 6, but continuous values of the KDE bandwidth p_{KDE} are obtained by morphing between templates obtained with other discrete values. The KDE bandwidth p_{KDE} is floating unconstrained in the fit as another parameter in the overall pass-fail ratio determined by the data.

The m_{red} and m_{J} distributions of the LL and TT regions of the fully-boosted analysis are shown in Figs. 1 and 2, respectively. Those for the semi-resolved analysis are shown in Fig. 3.

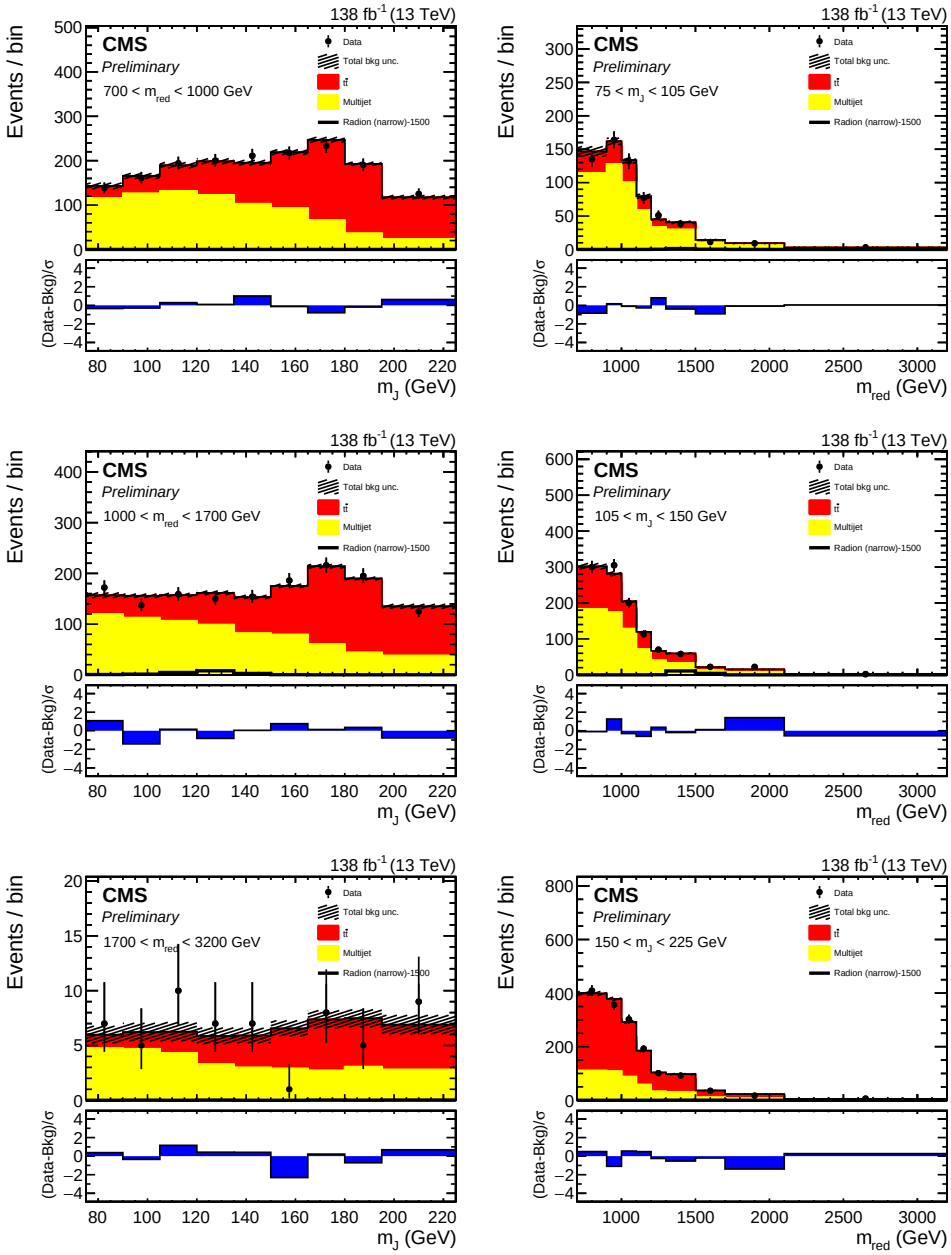

Figure 1: Slices of two-dimensional distributions of observed events and the post-fit templates in the LL pass region, projected onto the m_{J} (left) and m_{red} (right) axes, including expected radion signal at 1500 GeV. For this and following figures, the value of σ in the lower panel is $\sigma = \sqrt{\sigma_{bkg}^2 + \sigma_{data}^2}$.

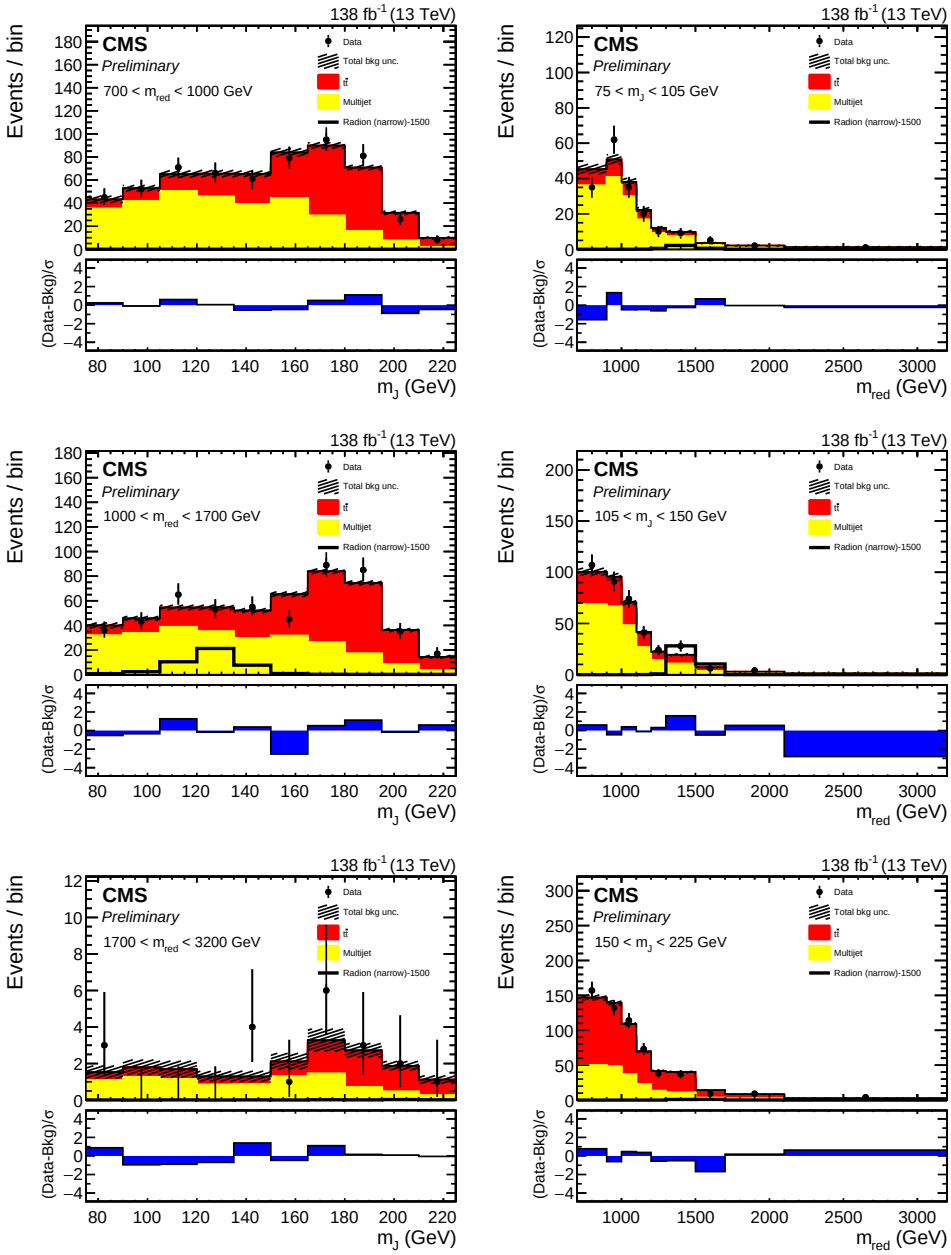

Figure 2: Slices of two-dimensional distributions of observed events and the post-fit templates in the TT pass region, projected onto the m_{J} (left) and m_{red} (right) axes, including expected radion signal at 1500 GeV.

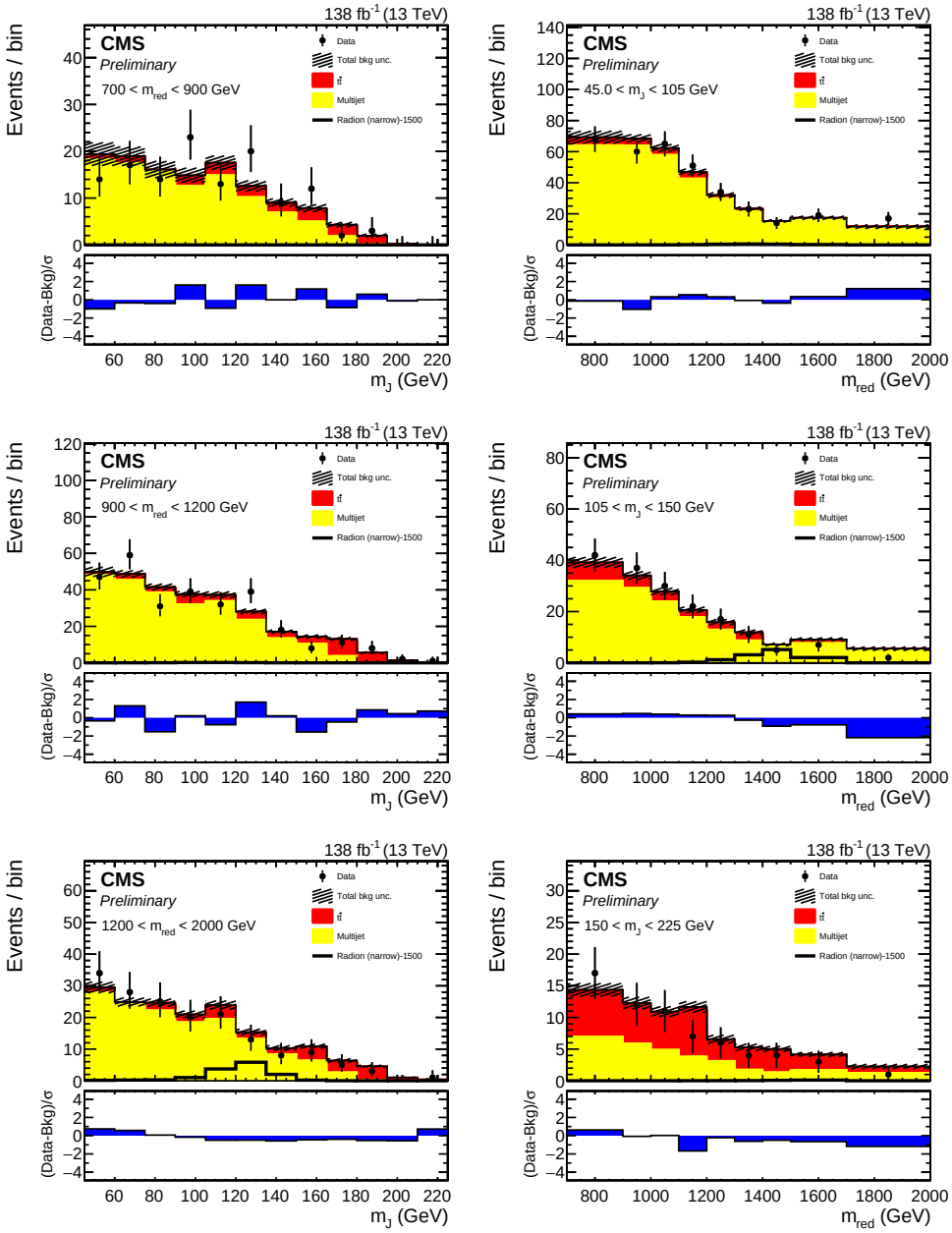

Figure 3: Slices of two-dimensional distributions of observed events and the post-fit templates in the TT pass region, projected onto the m_{J} (left) and m_{red} (right) axes, including expected radion signal at 1500 GeV.

6 Systematic uncertainties

The following sources of systematic uncertainty affect the expected signal and background event yields. None of these lead to a significant change in the signal shape. A complete list of systematic uncertainties is given in Table 3.

Table 3: Summary of the ranges of systematic uncertainties in the signal and background yields, for the combined fit of all ten regions for the radion resonance at 1500 GeV.

Source	uncertainty (Combined %)
Luminosity	1.3 %
Pileup	1–2 %
PDF and scales	0.5 %
$t\bar{t}$ cross section	5.0 %
Trigger efficiency	2.4 %
Top quark p_T re-weighting	0.2–1.5 %
DeepAK8 H $\to b\bar{b}$ efficiency	2.7 %
DeepAK8 $t\bar{t}$ efficiency	0.1 %
DeepJet b tagging efficiency	0.5 %
Jet energy scale and resolution	1 – 3 %
Jet mass scale and resolution	1 – 5 %
Trigger prefiring corrections (2016/2017)	0.5 %
KDE bandwidth	10 %
QCD multijet background fit	2-10 %

The uncertainties in the modelling of the trigger response are particularly important for $m_{\text{red}} < 1100\,\text{GeV}$, where the trigger efficiency drops below 99%. The trigger efficiency in simulation is corrected by a scale factor, which has an uncertainty between 1 and 15%, attributable to the control trigger inefficiency and the sample size used.

The impact of the jet energy scale and resolution uncertainties [66] on the signal yields was estimated to be 1–3%, depending on the signal mass. The jet mass scale and resolution were measured using a sample of boosted $W \to q\bar{q}'$ jets in semileptonic $t\bar{t}$ events. The jet mass scale and resolution has a 2% effect on the signal yields because of a change in the mean of the H jet mass distribution. A correction factor is applied to account for the difference in the jet shower profile of $W \to q\bar{q}'$ and $H \to b\bar{b}$ decays, by comparing the ratio of the efficiency of H and W jets using the PYTHIA 8 and HERWIG++ shower generators. This uncertainty, the H tagging correction factor, averages to 0.1%, depending on the resonance mass m_X.

Scale factors are used to correct the signal events yields so their double-b tagger and DeepJet discriminator efficiencies are the same as for data. The double-b tagger and the DeepJet discriminator scale factors are taken to be 100% correlated. The associated uncertainty is 2–9% [67], depending on the double-b tagger and requirement threshold and jet p_T, and is propagated to the total uncertainty in the signal yield.

The impact of the theoretical scale uncertainties and PDF uncertainties, the latter derived using the PDF4LHC procedure [49] and the NNPDF3.0 PDF sets, is estimated to be 0.5%. These uncertainties affect the product of the signal acceptance and the selection efficiency. The scale

and the PDF uncertainties have negligible impact on the signal m_{red} distributions. Additional systematic uncertainties associated with the pileup modelling (1–2%, based on a 4.6% variation on the pp total inelastic cross section) and with the integrated luminosity determination (2.5%) [59], are applied to the signal yield.

The systematic uncertainty applied to the signal is also applied to the $\mathrm{t\bar{t}}$+jets background, as appropriate. The total uncertainty in the $\mathrm{t\bar{t}}$+jets background is 7 %.

An additional uncertainty in the bandwidth parameter of the KDE algorithm, which acts as a scale for the width of the adaptive kernels, is accounted for by varying the parameter by unity.

The main source of uncertainty for the multijet background is due to the statistical uncertainty in the fit to the $R_{\mathrm{p/f}}$ ratio performed in the H jet mass sidebands. This uncertainty, amounting to 2–10%, is fully correlated between all m_{red} bins. Additional statistical uncertainties in the background shape and yield in the signal region result from the finite statistics of the multijets samples in the fail region and are evaluated using the Barlow–Beeston Lite method [68, 69]. These uncertainties are small as compared with the uncertainty in the $R_{\mathrm{p/f}}$ ratio, and are uncorrelated from bin to bin.

7 Results

We search for the bulk graviton and the radion with masses between 1 and 3 TeV. We use the scenario of Ref. [70] to describe the KK graviton, where the propagation of SM fields is allowed in the bulk and follows the characteristics of the SM gauge group, with the right-handed top quark localized near the TeV brane. The radion is an additional element of WED models that is needed to stabilize the size of the extra dimension l. The theoretical cross sections for $\sigma(\mathrm{pp} \to \mathrm{X})B(\mathrm{X} \to \mathrm{b\bar{b}b\bar{b}})$ are calculated using $\kappa/\overline{M_{\mathrm{Pl}}} = 0.5$ for the bulk gravitons and $\Lambda_{\mathrm{R}} = 3\,\mathrm{TeV}$ for the radions, of different masses. For these values of $\kappa/\overline{M_{\mathrm{Pl}}}$ and Λ_{R}, the branching fractions $\mathcal{B}(\mathrm{X} \to \mathrm{b\bar{b}b\bar{b}})$ are 10 and 23%, for the graviton and the radion, respectively [71].

Results are obtained using a statistical combination of the semi-resolved and fully-merged event categories. An $X \to \mathrm{HH}$ signal is resonant in the 2D space of the different signal event categories, as discussed in Section 5. The likelihood is formed by combining two-dimensional binned likelihoods of ten regions: TT, LL, and semi-resolved signal categories, and TT and LL $\mathrm{t\bar{t}}$ control categories, where each category provides both pass and fail region. The projections of 2D distributions in the five pass regions are shown in Figs. 1 through 3. The three signal regions are examined for an excess of events above the predicted background, and the data were found to be consistent with the expected background predictions.

Upper limits at 95% confidence level are set on the product of the production cross section and the branching fractions $\sigma(\mathrm{pp} \to \mathrm{X})\mathcal{B}(\mathrm{X} \to \mathrm{b\bar{b}b\bar{b}})$. They are obtained using the profile likelihood as a test statistic [72]. The systematic uncertainties are treated as nuisance parameters and are profiled in the minimization of the negative of the logarithm of the profile likelihood ratio and the distributions of the likelihood ratio are calculated using the asymptotic approximation [73] of the procedure reported in Refs. [74, 75]. As shown in Fig. 4, left, a narrow radion with mass between 1000 and 2600 GeV is excluded at 95% confidence level for $\Lambda_{\mathrm{R}} = 3\,\mathrm{TeV}$. Narrow bulk graviton for $k/\overline{M_{\mathrm{Pl}}} = 0.5$ is excluded at 95% confidence level only for masses between 1000 and 1200 GeV, as shown in Fig. 4, right. The deviation in observed limit at 1300 and 1500 GeV resonance masses is driven by an upward fluctuation of data over the background prediction at $m_{\mathrm{red}} \sim 1400$ GeV, as can be seen in Fig. 2, middle row. The expected limits are reported in Tables 4 and 5 for radions and bulk gravitons of different assumed masses, respectively.

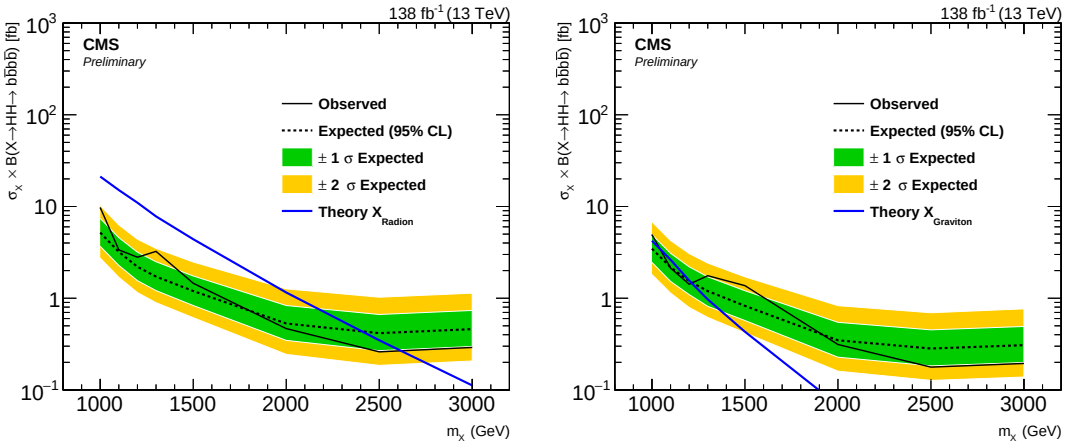

Figure 4: Upper limits at 95% confidence level on $\sigma(\mathrm{pp} \to \mathrm{X})\mathcal{B}(\mathrm{X} \to \mathrm{b\bar{b}b\bar{b}})$ for the narrow spin-0 radion (left) and the spin-2 bulk graviton (right) models. The predicted theoretical cross sections for the narrow radion and bulk graviton are also shown.

Table 4: Radion observed 95% CL exclusion limits.

Mass (GeV)	Obs. (fb)	Exp. lim. (fb)	+Exp (68%) (fb)	−Exp (68%) (fb)	+Exp (95%) (fb)	−Exp (95%) (fb)
1000	9.74	5.12	7.41	3.68	10.26	2.74
1100	3.37	3.20	4.58	2.28	6.31	1.69
1200	2.80	2.20	3.18	1.55	4.40	1.15
1300	3.24	1.72	2.50	1.21	3.5	0.89
1500	1.46	1.10	1.75	0.83	2.48	0.61
2000	0.47	0.53	0.83	0.34	1.26	0.24
2500	0.26	0.42	0.66	0.26	1.02	0.18
3000	0.29	0.46	0.74	0.29	1.13	0.20

Table 5: Graviton observed 95% CL exclusion limits.

Mass (GeV)	Obs. (fb)	Exp. lim. (fb)	+Exp (68%) (fb)	−Exp (68%) (fb)	+Exp (95%) (fb)	−Exp (95%) (fb)
1000	4.94	3.47	4.93	2.46	6.82	1.81
1100	2.13	2.12	3.10	1.52	4.26	1.14
1200	1.42	1.54	2.20	1.10	3.07	0.79
1300	1.76	1.20	1.71	0.82	2.42	0.62
1500	1.37	0.83	1.21	0.57	1.71	0.42
2000	0.31	0.35	0.55	0.23	0.83	0.16
2500	0.18	0.28	0.45	0.18	0.69	0.13
3000	0.19	0.31	0.49	0.20	0.77	0.14

8 Summary

A search is presented for the pair production of standard model Higgs bosons (HH), both decaying to a bottom quark-antiquark pair ($b\bar{b}$), using data from proton-proton collisions at a centre-of-mass energy of 13 TeV and corresponding to an integrated luminosity of 138 fb^{-1}. The search is conducted in the region of phase space where at least one of the Higgs bosons has a large Lorentz boost, so that the $H \to b\bar{b}$ decay products are collimated to form a single H jet. The search combines events with one H jet plus two b jets with events having two H jets, thus adding sensitivity to the previous analysis [32].

The results of the search are compared with predictions for the resonant production of a narrow Kaluza–Klein bulk graviton and a narrow radion in warped extradimensional models. The search is also sensitive to several beyond standard model non-resonant HH production scenarios. Such cases may arise either when an off-shell massive resonance produced in proton-proton collisions decays to HH, or through beyond standard model effects in the Higgs boson coupling parameters. The results are interpreted in terms of upper limits on the product of the cross section for the respective signal processes and the branching fraction to $HH \to b\bar{b}b\bar{b}$, at 95% confidence level.

The upper limits range from 4.94 to 0.19 fb for the bulk graviton and from 9.74 to 0.29 fb for the radion for the mass range 1–3 TeV.

References

[1] ATLAS Collaboration, "Observation of a new particle in the search for the standard model Higgs boson with the ATLAS detector at the LHC", *Phys. Lett. B* **716** (2012) 01, doi:10.1016/j.physletb.2012.08.020, arXiv:1207.7214.

[2] CMS Collaboration, "Observation of a new boson at a mass of 125 GeV with the CMS experiment at the LHC", *Phys. Lett. B* **716** (2012) 30, doi:10.1016/j.physletb.2012.08.021, arXiv:1207.7235.

[3] CMS Collaboration, "Observation of a new boson with mass near 125 GeV in pp collisions at $\sqrt{s}$ = 7 and 8 TeV", *JHEP* **06** (2013) 081, doi:10.1007/JHEP06(2013)081, arXiv:1303.4571.

[4] D. de Florian et al., "Handbook of LHC Higgs cross sections: 4. deciphering the nature of the Higgs sector", CERN Report CERN-2017-002-M, CERN, 2016. doi:10.23731/CYRM-2017-002, arXiv:1610.07922.

[5] D. de Florian and J. Mazzitelli, "Higgs boson pair production at next-to-next-to-leading order in QCD", *Phys. Rev. Lett.* **111** (2013) 201801, doi:10.1103/PhysRevLett.111.201801, arXiv:1309.6594.

[6] J. Baglio et al., "The measurement of the Higgs self-coupling at the LHC: theoretical status", *JHEP* **04** (2013) 151, doi:10.1007/JHEP04(2013)151, arXiv:1212.5581.

[7] L. Randall and R. Sundrum, "A large mass hierarchy from a small extra dimension", *Phys. Rev. Lett.* **83** (1999) 3370, doi:10.1103/PhysRevLett.83.3370, arXiv:hep-ph/9905221.

[8] R. Grober and M. Muhlleitner, "Composite Higgs boson pair production at the LHC", *JHEP* **06** (2011) 020, doi:10.1007/JHEP06(2011)020, arXiv:1012.1562.

[9] W. D. Goldberger and M. B. Wise, "Modulus stabilization with bulk fields", *Phys. Rev. Lett.* **83** (1999) 4922, doi:10.1103/PhysRevLett.83.4922, arXiv:hep-ph/9907447.

[10] O. DeWolfe, D. Z. Freedman, S. S. Gubser, and A. Karch, "Modeling the fifth dimension with scalars and gravity", *Phys. Rev. D* **62** (2000) 046008, doi:10.1103/PhysRevD.62.046008, arXiv:hep-th/9909134.

[11] C. Csaki, M. Graesser, L. Randall, and J. Terning, "Cosmology of brane models with radion stabilization", *Phys. Rev. D* **62** (2000) 045015, doi:10.1103/PhysRevD.62.045015, arXiv:hep-ph/9911406.

[12] H. Davoudiasl, J. L. Hewett, and T. G. Rizzo, "Phenomenology of the Randall-Sundrum gauge hierarchy model", *Phys. Rev. Lett.* **84** (2000) 2080, doi:10.1103/PhysRevLett.84.2080, arXiv:hep-ph/9909255.

[13] C. Csaki, M. L. Graesser, and G. D. Kribs, "Radion dynamics and electroweak physics", *Phys. Rev. D* **63** (2001) 065002, doi:10.1103/PhysRevD.63.065002, arXiv:hep-th/0008151.

[14] K. Agashe, H. Davoudiasl, G. Perez, and A. Soni, "Warped gravitons at the LHC and beyond", *Phys. Rev. D* **76** (2007) 036006, doi:10.1103/PhysRevD.76.036006, arXiv:hep-ph/0701186.

[15] G. F. Giudice, R. Rattazzi, and J. D. Wells, "Graviscalars from higher dimensional metrics and curvature Higgs mixing", *Nucl. Phys. B* **595** (2001) 250, doi:10.1016/S0550-3213(00)00686-6, arXiv:hep-ph/0002178.

[16] ATLAS Collaboration, "Search for Higgs boson pair production in the $\gamma\gamma b\bar{b}$ final state using pp collision data at $\sqrt{s} = 8$ TeV from the ATLAS detector", *Phys. Rev. Lett.* **114** (2015) 081802, doi:10.1103/PhysRevLett.114.081802, arXiv:1406.5053.

[17] ATLAS Collaboration, "Search for Higgs boson pair production in the $b\bar{b}b\bar{b}$ final state from pp collisions at $\sqrt{s} = 8$ TeV with the ATLAS detector", *Eur. Phys. J. C* **75** (2015) 412, doi:10.1140/epjc/s10052-015-3628-x, arXiv:1506.00285.

[18] ATLAS Collaboration, "Searches for Higgs boson pair production in the $HH \to b\bar{b}\tau\tau$, $\gamma\gamma WW^*$, $\gamma\gamma b\bar{b}$, $b\bar{b}b\bar{b}$ channels with the ATLAS detector", *Phys. Rev. D* **92** (2015) 092004, doi:10.1103/PhysRevD.92.092004, arXiv:1509.04670.

[19] ATLAS Collaboration, "Search for pair production of Higgs bosons in the $b\bar{b}b\bar{b}$ final state using proton–proton collisions at $\sqrt{s} = 13$ TeV with the ATLAS detector", *Phys. Rev. D* **94** (2016) 052002, doi:10.1103/PhysRevD.94.052002, arXiv:1606.04782.

[20] ATLAS Collaboration, "Search for pair production of Higgs bosons in the $b\bar{b}b\bar{b}$ final state using proton-proton collisions at $\sqrt{s} = 13$ TeV with the ATLAS detector", *JHEP* **01** (2019) 030, doi:10.1007/JHEP01(2019)030, arXiv:1804.06174.

[21] ATLAS Collaboration, "Search for Resonant and Nonresonant Higgs Boson Pair Production in the $b\bar{b}\tau^+\tau^-$ Decay Channel in pp Collisions at $\sqrt{s} = 13$ TeV with the ATLAS Detector", *Phys. Rev. Lett.* **121** (2018) 191801, doi:10.1103/PhysRevLett.121.191801, arXiv:1808.00336.

[22] ATLAS Collaboration, "Search for Higgs boson pair production in the $\gamma\gamma b\bar{b}$ final state with 13 TeV pp collision data collected by the ATLAS experiment", *JHEP* **11** (2018) 040, doi:10.1007/JHEP11(2018)040, arXiv:1807.04873.

[23] CMS Collaboration, "Searches for heavy Higgs bosons in two-Higgs-doublet models and for $t \to ch$ decay using multilepton and diphoton final states in pp collisions at 8 TeV", *Phys. Rev. D* **90** (2014) 112013, doi:10.1103/PhysRevD.90.112013, arXiv:1410.2751.

[24] CMS Collaboration, "Search for Higgs boson pair production in the $b\bar{b}\tau\tau$ final state in proton-proton collisions at $\sqrt{s} = 8$ TeV", *Phys. Rev. D* **96** (2017) 072004, doi:10.1103/PhysRevD.96.072004, arXiv:1707.00350.

[25] CMS Collaboration, "Search for resonant pair production of Higgs bosons decaying to two bottom quark-antiquark pairs in proton-proton collisions at 8 TeV", *Phys. Lett. B* **749** (2015) 560, doi:10.1016/j.physletb.2015.08.047, arXiv:1503.04114.

[26] CMS Collaboration, "Searches for a heavy scalar boson H decaying to a pair of 125 GeV Higgs bosons hh or for a heavy pseudoscalar boson A decaying to Zh, in the final states with $h \to \tau\tau$", *Phys. Lett. B* **755** (2016) 217, doi:10.1016/j.physletb.2016.01.056, arXiv:1510.01181.

[27] CMS Collaboration, "Search for two Higgs bosons in final states containing two photons and two bottom quarks in proton-proton collisions at 8 TeV", *Phys. Rev. D* **94** (2016) 052012, doi:10.1103/PhysRevD.94.052012, arXiv:1603.06896.

[28] CMS Collaboration, "Search for heavy resonances decaying to two Higgs bosons in final states containing four b quarks", *Eur. Phys. J. C* **76** (2016) 371, doi:10.1140/epjc/s10052-016-4206-6, arXiv:1602.08762.

[29] CMS Collaboration, "Search for Higgs boson pair production in events with two bottom quarks and two tau leptons in proton-proton collisions at $\sqrt{s} = 13$ TeV", *Phys. Lett. B* **778** (2018) 101, doi:10.1016/j.physletb.2018.01.001, arXiv:1707.02909.

[30] CMS Collaboration, "Search for resonant and nonresonant Higgs boson pair production in the $b\bar{b}\ell\nu\ell\nu$ final state in proton-proton collisions at $\sqrt{s} = 13$ TeV", *JHEP* **01** (2018) 054, doi:10.1007/JHEP01(2018)054, arXiv:1708.04188.

[31] CMS Collaboration, "Search for Higgs boson pair production in the $\gamma\gamma b\bar{b}$ final state in pp collisions at $\sqrt{s} = 13$ TeV", *Phys. Lett. B* **788** (2019) 7, doi:10.1016/j.physletb.2018.10.056, arXiv:1806.00408.

[32] CMS Collaboration, "Search for a massive resonance decaying to a pair of Higgs bosons in the four b quark final state in proton-proton collisions at $\sqrt{s} = 13$ TeV", *Phys. Lett. B* **781** (2018) 244, doi:10.1016/j.physletb.2018.03.084, arXiv:1710.04960.

[33] CMS Collaboration, "Search for resonant pair production of Higgs bosons decaying to bottom quark-antiquark pairs in proton-proton collisions at 13 TeV", *JHEP* **08** (2018) 152, doi:10.1007/JHEP08(2018)152, arXiv:1806.03548.

[34] M. Gouzevitch et al., "Scale-invariant resonance tagging in multijet events and new physics in Higgs pair production", *JHEP* **07** (2013) 148, doi:10.1007/JHEP07(2013)148, arXiv:1303.6636.

[35] CMS Collaboration, "Search for production of Higgs boson pairs in the four b quark final state using large-area jets in proton-proton collisions at $\sqrt{s} = 13$ TeV", *JHEP* **01** (2019) 040, doi:10.1007/JHEP01(2019)040, arXiv:1808.01473.

[36] CMS Collaboration, "The CMS experiment at the CERN LHC", *JINST* **3** (2008) S08004, doi:10.1088/1748-0221/3/08/S08004.

[37] CMS Collaboration, "The CMS trigger system", *JINST* **12** (2017) P01020, doi:10.1088/1748-0221/12/01/P01020, arXiv:1609.02366.

[38] CMS Trigger, Data Acquisition Group Collaboration, "The CMS high level trigger", *Eur. Phys. J. C* **46** (2006) 605, doi:10.1140/epjc/s2006-02495-8, arXiv:hep-ex/0512077.

[39] CMS Collaboration, "Particle-flow reconstruction and global event description with the cms detector", *JINST* **12** (2017) P10003, doi:10.1088/1748-0221/12/10/P10003, arXiv:1706.04965.

[40] M. Cacciari, G. P. Salam, and G. Soyez, "The anti-k_{T} jet clustering algorithm", *JHEP* **04** (2008) 063, doi:10.1088/1126-6708/2008/04/063, arXiv:0802.1189.

[41] M. Cacciari, G. P. Salam, and G. Soyez, "FastJet user manual", *Eur. Phys. J. C* **72** (2012) 1896, doi:10.1140/epjc/s10052-012-1896-2, arXiv:1111.6097.

[42] CMS Collaboration, "Jet energy scale and resolution in the CMS experiment in pp collisions at 8 TeV", *JINST* **12** (2017) P02014, doi:10.1088/1748-0221/12/02/P02014, arXiv:1607.03663.

[43] CMS Collaboration, "Performance of missing transverse momentum reconstruction in proton-proton collisions at $\sqrt{s} = 13$ TeV using the CMS detector", *JINST* **14** (2019) P07004, doi:10.1088/1748-0221/14/07/P07004, arXiv:1903.06078.

[44] J. Alwall et al., "The automated computation of tree-level and next-to-leading order differential cross sections, and their matching to parton shower simulations", *JHEP* **07** (2014) 079, doi:10.1007/JHEP07(2014)079, arXiv:1405.0301.

[45] NNPDF Collaboration, "Parton distributions for the LHC Run II", *JHEP* **04** (2015) 040, doi:10.1007/JHEP04(2015)040, arXiv:1410.8849.

[46] L. A. Harland-Lang, A. D. Martin, P. Motylinski, and R. S. Thorne, "Parton distributions in the LHC era: MMHT 2014 PDFs", *Eur. Phys. J. C* **75** (2015) 204, doi:10.1140/epjc/s10052-015-3397-6, arXiv:1412.3989.

[47] A. Buckley et al., "LHAPDF6: parton density access in the LHC precision era", *Eur. Phys. J. C* **75** (2015) 132, doi:10.1140/epjc/s10052-015-3318-8, arXiv:1412.7420.

[48] S. Carrazza, J. I. Latorre, J. Rojo, and G. Watt, "A compression algorithm for the combination of PDF sets", *Eur. Phys. J. C* **75** (2015) 474, doi:10.1140/epjc/s10052-015-3703-3, arXiv:1504.06469.

[49] J. Butterworth et al., "PDF4LHC recommendations for LHC Run II", *J. Phys. G* **43** (2016) 023001, doi:10.1088/0954-3899/43/2/023001, arXiv:1510.03865.

[50] T. Sjöstrand et al., "An Introduction to PYTHIA 8.2", *Comput. Phys. Commun.* **191** (2015) 159, doi:10.1016/j.cpc.2015.01.024, arXiv:1410.3012.

[51] S. Frixione, G. Ridolfi, and P. Nason, "A positive-weight next-to-leading-order Monte Carlo for heavy flavour hadroproduction", *JHEP* **09** (2007) 126, doi:10.1088/1126-6708/2007/09/126, arXiv:0707.3088.

[52] S. Frixione, P. Nason, and C. Oleari, "Matching NLO QCD computations with parton shower simulations: the POWHEG method", *JHEP* **11** (2007) 070, doi:10.1088/1126-6708/2007/11/070, arXiv:0709.2092.

[53] S. Alioli, P. Nason, C. Oleari, and E. Re, "A general framework for implementing NLO calculations in shower Monte Carlo programs: the POWHEG BOX", *JHEP* **06** (2010) 043, doi:10.1007/JHEP06(2010)043, arXiv:1002.2581.

[54] P. Skands, S. Carrazza, and J. Rojo, "Tuning Pythia 8.1: the Monash 2013 tune", *Eur. Phys. J. C* **74** (2014) 3024, doi:10.1140/epjc/s10052-014-3024-y, arXiv:1404.5630.

[55] CMS Collaboration, "Measurement of the top quark mass with lepton+jets final states using pp collisions at $\sqrt{s} = 13\,\text{TeV}$", *Eur. Phys. J. C* **78** (2018) 891, doi:10.1140/epjc/s10052-018-6332-9, arXiv:1805.01428.

[56] M. Czakon and A. Mitov, "Top++: A program for the calculation of the top-pair cross-section at hadron colliders", *Comput. Phys. Commun.* **185** (2014) 2930, doi:10.1016/j.cpc.2014.06.021, arXiv:1112.5675.

[57] GEANT4 Collaboration, "GEANT4—a simulation toolkit", *Nucl. Instrum. Meth. A* **506** (2003) 250, doi:10.1016/S0168-9002(03)01368-8.

[58] J. Allison et al., "Geant4 developments and applications", *IEEE Trans. Nucl. Sci.* **53** (2006) 270, doi:10.1109/TNS.2006.869826.

[59] CMS Collaboration, "Measurement of the inelastic proton-proton cross section at $\sqrt{s} = 13\,\text{TeV}$", *JHEP* **07** (2018) 161, doi:10.1007/JHEP07(2018)161, arXiv:1802.02613.

[60] D. Krohn, J. Thaler, and L.-T. Wang, "Jet trimming", *JHEP* **02** (2010) 084, doi:10.1007/JHEP02(2010)084, arXiv:0912.1342.

[61] M. Dasgupta, A. Fregoso, S. Marzani, and G. P. Salam, "Towards an understanding of jet substructure", *JHEP* **09** (2013) 029, doi:10.1007/JHEP09(2013)029, arXiv:1307.0007.

[62] A. J. Larkoski, S. Marzani, G. Soyez, and J. Thaler, "Soft drop", *JHEP* **05** (2014) 146, doi:10.1007/JHEP05(2014)146, arXiv:1402.2657.

[63] ATLAS and CMS Collaborations, "Combined measurement of the Higgs boson mass in pp collisions at $\sqrt{s} = 7$ and 8 tev with the ATLAS and CMS experiments", *Phys. Rev. Lett.* **114** (2015) 191803, doi:10.1103/PhysRevLett.114.191803, arXiv:1503.07589.

[64] CMS Collaboration, "Measurements of properties of the Higgs boson decaying into the four-lepton final state in pp collisions at $\sqrt{s} = 13\,\text{TeV}$", *JHEP* **11** (2017) 047, doi:10.1007/JHEP11(2017)047, arXiv:1706.09936.

[65] K. S. Cranmer, "Kernel estimation in high-energy physics", *Comput. Phys. Commun.* **136** (2001) 198–207, doi:10.1016/S0010-4655(00)00243-5, arXiv:hep-ex/0011057.

[66] CMS Collaboration, "Jet algorithms performance in 13 TeV data", CMS Physics Analysis Summary CMS-PAS-JME-16-003, CERN, 2017.

[67] CMS Collaboration, "Identification of heavy-flavour jets with the CMS detector in pp collisions at 13 TeV", *JINST* **13** (2017) P05011, doi:10.1088/1748-0221/13/05/P05011, arXiv:1712.07158.

[68] R. Barlow and C. Beeston, "Fitting using finite Monte Carlo samples", *Comput. Phys. Commun.* **77** (1993) 219, doi:10.1016/0010-4655(93)90005-W.

[69] J. S. Conway, "Incorporating nuisance parameters in likelihoods for multisource spectra", in *Proceedings, PHYSTAT 2011 Workshop on Statistical Issues Related to Discovery Claims in Search Experiments and Unfolding, CERN, Geneva, Switzerland 17-20 January 2011*, p. 115. 2011. arXiv:1103.0354. doi:10.5170/CERN-2011-006.115.

[70] A. L. Fitzpatrick, J. Kaplan, L. Randall, and L.-T. Wang, "Searching for the Kaluza-Klein graviton in bulk RS models", *JHEP* **09** (2007) 013, doi:10.1088/1126-6708/2007/09/013, arXiv:hep-ph/0701150.

[71] A. Oliveira, "Gravity particles from warped extra dimensions, predictions for LHC", 2014. arXiv:1404.0102.

[72] ATLAS and CMS Collaborations, The LHC Higgs Combination Group, "Procedure for the LHC Higgs boson search combination in Summer 2011", Technical Report CMS-NOTE-2011-005. ATL-PHYS-PUB-2011-11, CERN, 2011.

[73] G. Cowan, K. Cranmer, E. Gross, and O. Vitells, "Asymptotic formulae for likelihood-based tests of new physics", *Eur. Phys. J. C* **71** (2011) 1554, doi:10.1140/epjc/s10052-011-1554-0, arXiv:1007.1727. [Erratum: doi:10.1140/epjc/s10052-013-2501-z].

[74] A. L. Read, "Presentation of search results: The CL_s technique", *J. Phys. G* **28** (2002) 2693, doi:10.1088/0954-3899/28/10/313.

[75] T. Junk, "Confidence level computation for combining searches with small statistics", *Nucl. Instrum. Meth. A* **434** (1999) 435, doi:10.1016/S0168-9002(99)00498-2, arXiv:hep-ex/9902006.